Robust Blind Deconvolution Using Relative Total Variation as a Regularization Penalty

Yunzhi Lin[1(✉)] and Wenze Shao[2,3]

[1] School of Automation, Southeast University, Nanjing 210096, China
linyunzhi1996@126.com
[2] College of Telecommunications and Information Engineering, Nanjing University of Posts and Telecommunications, Nanjing 210003, China
shaowenze1010@163.com
[3] National Engineering Research Center of Communications and Networking, Nanjing University of Posts and Telecommunications, Nanjing 210003, China

Abstract. Blind image deblurring or deconvolution is a very hot topic towards which numerous methods have been put forward in the past decade, demonstrating successful deblurring results on one or another benchmark natural image dataset. However, most of existing algorithms are found not robust enough as dealing with images in specific scenarios, such as images with text, saturated area or face. In this paper, a robust blind deblurring approach is presented using relative total variation as a regularization penalty. To the best of our knowledge, none of previous studies have followed this modeling principle. The underlying idea is to pursue more accurate intermediate image for more reliable kernel estimation by harnessing relative total variation which could extract salient structures from textures and suppress ringing artifacts and noise as well. An iterative estimating algorithm is finally deduced for alternatively update of sharp image and blur kernel by operator splitting and augmented Lagrangian. Extensive experiments on a challenging synthetic dataset and real-world images as well are conducted to validate the new method with comparison against the state-of-the-art approaches from 2006 to 2014. Based on both PSNR and SSIM and a non-reference evaluation metric, the results demonstrate that our approach is comparatively more effective to process blurred images in more challenging scenarios.

Keywords: Blind deblurring · Motion blur · Kernel estimation
Image restoration

1 Introduction

Motion blur is an artifact caused by the movement of the camera sensor during the exposure, which leads to significant information loss of the picture. This problem has been increasingly important since the widespread use of the hand-held cameras, particularly the smart phones.

S. Satoh (Ed.): PSIVT 2017, LNCS 10799, pp. 325–337, 2018.
https://doi.org/10.1007/978-3-319-92753-4_26

Generally, based on the assumption that the motion blur is shift-invariant, the blur process could be modeled as follows:

$$y = k * x + n \tag{1}$$

where x is the latent sharp image, k is the blur kernel, n is the image noise, $*$ denotes convolution and y is the observed blur image.

Thus, motion deblurring could be simplified to a blind deconvolution task, i.e., recovering both the latent image x and the kernel k from the observed blurry image y. It is apparent that the task is mathematically an ill-posed problem since different sharp images in combination with distinct blur kernels may produce the same blurry images. Nowadays, most existing methods are formulated in the Bayesian framework to solve this problem, specifically including two inference principles: Variational Bayes (VB) and Maximum a Posteriori (MAP). The proposed approach in this paper falls into the MAP considering its flexibility in both modeling and inference.

Recent years has witnessed much progress in blind image deblurring. One group of researchers [1, 2, 4, 7–11, 22, 24] concentrates on seeking appropriate sparse priors of x and k. Another group [12–14] combines the salient edge selection with simple Gaussian prior to speed up the computational process. Although many approaches seem to perform well on some particular dataset, e.g., provided by Fergus et al. [1], Levin et al. [2], they usually fail in getting satisfying results under more complex situations, such as images of text, face, natural environment, or dark scenes with light saturation. The recent comprehensive comparative study [5] has showed that the state-of-the-art approaches from 2006 to 2014 are not robust enough to suit all these cases.

In this paper, a robust blind deblurring approach is presented using relative total variation as a regularization penalty. Relative Total Variation (RTV) proposed by Xu et al. [3] is a tricky yet interesting method to extract salient structures from the image. To the best of our knowledge, none of previous studies have followed this modeling principle. The underlying idea is to pursue more accurate intermediate latent image x for reliable kernel estimation by harnessing RTV which may extract salient structures from textures and suppress ringing artifacts and noise as well. To be noted that, as in Cho et al. [12] and Xu and Jia [13] edge enhancing via shock filtering is also adopted during updating the latent image x. In the blur kernel estimation stage, an L0-L2 prior is imposed on the kernel just following one of our previous work [11] which is found adapt the proposed approach in this paper quite well. With above modeling processes, an iterative estimating algorithm is finally deduced for update of sharp image and blur kernel in an alternative manner by operator splitting and augmented Lagrangian. With estimated blur kernel, a non-blind deconvolution developed from the hyper-Laplacian prior [4] is adopted for the final restoration of the clear image. Extensive experiments on a comprehensive synthetic dataset including text, face and low illumination images and real-world images as well are conducted to validate the new method with comparison against the state-of-the-art approaches from 2006 to 2014. Based on both PSNR and SSIM and a non-reference evaluation metric [6] developed from the massive user study, the results demonstrate that our approach is comparatively more effective to process blurred images in more challenging scenarios.

2 Related Work

To solve the ill-posed problem of blind deconvolution, many previous methods employ multi-scale framework and impose constraints on not only the latent image but also blur kernel. For example, Fergus et al. [1] used a variational Bayesian method with a mixture of Gaussians and exponential prior on the image and kernel respectively. However, this statistical model is of great complexity and the resulting algorithm is vulnerable to noise. Shan et al. [7] proposed a piece-wise prior to satisfy the natural power-law of the image. Nevertheless, the deblurring results were much smooth and had many artifacts. Similarly, Krishnan et al. [8] introduced a normalized L1/L2 prior to distinguish the sharp image from the blurry one. However, the authors' claimed discrimination is questionable since L1/L2 is found fail in distinguishing many natural images. Lately, the L0 prior has proven to be the most efficient sparse prior. Xu et al. [9] first applied the L0 gradient prior to the estimation of latent image. Then Pan et al. [10] applied the L0 priors on both the gradient and intensity domains to the text image. Shao et al. [11] proposed an easy-to-implement and effective bi-L0-L2 prior on both the sharp image and blur kernel. While these algorithms obtain good results on one or another particular dataset, their performance is not robust enough to adapt diverse imaging scenarios. Recently, Pan et al. [18] further proposed to apply the L0 priors on both the gradient domain and the dark channel and achieved improved deblurring performance.

To avoid the negative influence of the textures or saturated areas on kernel estimation, another group of researchers employs smoothing/enhancing filters for salient edge selection. For example, Cho et al. [12] used bilateral filter and shocking filter; Xu and Jia [13] applied Gaussian filter and shocking filter, together with the Iterative Support Detection (ISD) to select salient edges. Recently, Pan et al. [14] proposed to remove the outliers in the saturated area to optimize the kernel estimation.

There are also studies making contributions to other aspects of motion deblurring. Whyte et al. [15] proposed a geometrically consistent model to take non-uniform blur into consideration. However, their performance is not satisfying within synthetic uniform dataset. Hu and Yang [16] selected a best region patch instead of the whole image for kernel estimation. Hu et al. [17] also used light streaks to predict the kernel in the dark scenario. While these novel algorithms expand the existing methods, none of them are competitive compared against other state-of-the-art approaches as surveyed in [5].

3 Robust Blind Kernel Estimation

In this section, we present a robust approach with RTV as the regularization term on the latent image x, combined with salient edge selection and L0-L2-norm regularized kernel estimation.

Following model (1), the basic cost function of our method is formulated as

$$\min_{x,k} \lambda \|k * x - y\|^2 + \alpha_x R_x(x) + \alpha_k R_k(k) \tag{2}$$

where $\lambda, \alpha_x, \alpha_k$, are the positive weights; $R_x(x), R_k(k)$ represent the regularization term on x and k respectively. Then, x and k can be solved alternatively by minimizing (2). Figure 1 shows the flowchart of final algorithm including an outer iteration and two inner iterations as well as additional salient edge selection step. Besides, a coarse-to-fine manner is adopted for the sake of avoiding the local minima, which is a common routine in the MAP-based blind deconvolution [2].

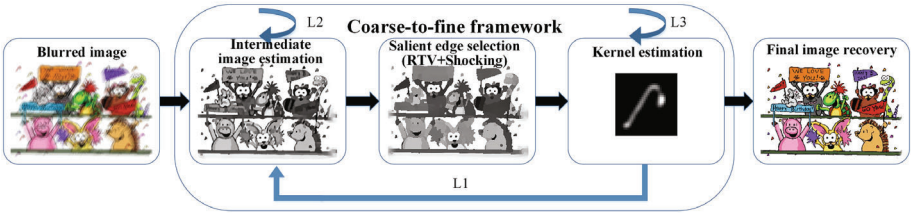

Fig. 1. Flowchart of the proposed method. L2 and L3 represent the inner iterations. L1 denotes the outer iterations and is implemented in a multi-scale (coarse-to-fine) framework.

3.1 Intermediate Latent Image Estimation

For the sake of clearness, the relative total variation is firstly introduced here which is proposed in [3], defined as

$$\sum_p \frac{D_{i,j}(p)}{L_{i,j}(p)+\varepsilon} = \sum_p \frac{\sum_{q(p)} g_{p,q}\left|(\partial_{i,j}x)_q\right|}{\left|\sum_{q\epsilon R(p)} g_{p,q}(\partial_{i,j}x)_q\right|+\varepsilon} \tag{3}$$

$$g_{p,q} \propto \exp\left(-\frac{(x_p-x_q)^2+(y_p-y_q)^2}{2\sigma^2}\right) \tag{4}$$

where i and j represent the horizontal and vertical direction respectively; q belongs to $R(p)$, the rectangle region centered at pixel p; ∂ denotes the partial derivative; $g_{p,q}$ is a correlation weighting function calculating the spatial affinity; ε specifies the maximum size of texture elements, we set it to 0.02 empirically; σ controls the spatial scale of the window.

Considering the MAP framework, we could obtain the intermediate image x by fixing the kernel k. By omitting the terms not involved in x, the intermediate image model is transformed to (5):

$$x_{i+1} = \arg\min_x \lambda\|k_i * x - y\|^2 + C_x^i \alpha_x \sum_p \frac{\sum_{q\epsilon R(p)} g_{p,q}\left|(\partial_{i,j}x)_q\right|}{\left|\sum_{q\epsilon R(p)} g_{p,q}(\partial_{i,j}x)_q\right|+\varepsilon} \tag{5}$$

where $0 \leq i \leq I-1$, I is the outer iteration number; $C_x^i < 1$ is a positive continuation factor which is fixed as 2/3. In this way, the weight of RTV prior diminishes as the process goes on, resulting in the cost function less constrained.

To solve problem (5), we first rewrite it into a matrix-vector form:

$$x_{i+1} = \arg\min_x \lambda \left\| K_i * x - V_y \right\|^2 + C_x^i \alpha_x \sum\nolimits_p \frac{\sum_{q \epsilon R(p)} g_{p,q} \left| (\partial_{i,j} x)_q \right|}{\left| \sum_{q \epsilon R(p)} g_{p,q} (\partial_{i,j} x)_q \right| + \varepsilon} \tag{6}$$

where $K \epsilon R^{M \times M}$ is the BCCB (block circulant matrix with circulant blocks) blurring matrix, M is the number of image pixels, and V_y is the vector representation of y. We adopt the well-known OSAL (operator splitting and augmented Lagrangian) scheme [11] to solve (6). An auxiliary variable u is introduced to substitute x, thus (6) written as

$$\begin{aligned} (x_i^{l+1}, u_i^{l+1}) = \arg\min_{x,u} \lambda \left\| K_i * x - V_y \right\|^2 + C_x^i \alpha_x \sum\nolimits_p \frac{\sum_{q \epsilon R(p)} g_{p,q} \left| (\partial_{i,j} u)_q \right|}{\left| \sum_{q \epsilon R(p)} g_{p,q} (\partial_{i,j} u)_q \right| + \varepsilon} \\ + C_x^i \mu_x^l (x-u) + C_x^i \tfrac{\gamma_x}{2} x - u^2 \end{aligned} \tag{7}$$

where $0 \leq l \leq P-1$, P is the inner iteration number; γ_x is a fixed parameter ensuring the similarity between x and u which is set to 100 empirically; and μ_x is the augmented Lagrangian penalty parameter which is updated as

$$\mu_x^{l+1} = \mu_x^l + \gamma_x \left(x_i^{l+1} - u_i^{l+1} \right) \tag{8}$$

When x is fixed, u could be solved by minimizing (9)

$$u_i^{l+1} = \arg\min_u \alpha_x \sum\nolimits_p \frac{\sum_{q \epsilon R(p)} g_{p,q} \left| (\partial_{i,j} x)_q \right|}{\left| \sum_{q \epsilon R(p)} g_{p,q} (\partial_{i,j} x)_q \right| + \varepsilon} + \frac{\gamma_x}{2} \left\| x + \frac{1}{\gamma_x} \mu_x^l - u \right\|^2 \tag{9}$$

Note that the form of (9) is similar to the cost function (10) in [3], i.e.,

$$\min_S \sum\nolimits_p \left(S_p - O_p \right)^2 + \lambda \left(\frac{D_x(p)}{L_x(p) + \varepsilon} + \frac{D_y(p)}{L_y(p) + \varepsilon} \right) \tag{10}$$

We just set the parameters in (10) as $\lambda = \frac{2a_x}{\gamma_x}$, $O = x + \frac{\mu_x^l}{\gamma_x}$, and (9) can be then solved exactly the same as in [3], i.e., in a plug-and-play manner.

Following (6), the intermediate image x can be solved with u provided,

$$\arg\min_x \frac{\lambda}{C_x^i} \left\| K_i * x - V_y \right\|^2 + \frac{\gamma_x}{2} \left\| x + \frac{1}{\gamma_x} \mu_x^l - u_i^l \right\|^2 \tag{11}$$

Due to the BCCB assumption over K_i, (11) can be efficiently solved by applying fast Fourier transform (FFT) based on the Paseval's theorem. The expression could be as follows:

$$x_i^{l+1} = \mathrm{F}^{-1}\left(\frac{\overline{\mathrm{F}(k_i)}_{\circ}\mathrm{F}(y) + \frac{C_x^i \gamma_x}{2\lambda}\mathrm{F}(u_i^l - \frac{1}{\gamma_x}\mu_x^l)}{\mathrm{F}(k_i)_{\circ}\overline{\mathrm{F}(k_i)} + \frac{C_x^i \gamma_x}{2\lambda}}\right) \tag{12}$$

where $\mathrm{F}(\cdot)$ and $\mathrm{F}^{-1}(\cdot)$ represent the FFT and the inverse FFT, respectively, $\overline{(\cdot)}$ denotes the conjugate operator and $\circ$ is an element-wise multiplication operator. Note that to reduce the ringing artifacts caused by implementation in the frequency domain, one way is to expand the image and taper discontinuities along image edges, which is a simple yet effective preconditioning step also mentioned in [1, 11].

3.2 Salient Edge Selection

Edge information is the key to estimate the kernel accurately. The principle has been validated by many papers [2, 12, 13], that a salient edge does not change much after the blur process. As Xu and Jia [13] pointed out, if the edge width is smaller than the kernel size, it may be weakened significantly, thus damaging the kernel estimation. However, previous edge selection methods have some drawbacks. The bilateral filter may weaken the salient edge and make them less robust. WLS filter [19] is too weak to remove the tiny small edges. Many of these edges still remain after the estimating process. Moreover, the approach of L0 gradient [20] could not effectively distinguish the small edges from the salient ones, thus removing too many edges. As a result, there are not enough salient edges for estimation.

We instead adopt the proposed Relative Total Variation (RTV) method [3] to finish the task. It is found that these small edges often exist in the form of texture in the image. Thus, RTV is the best method to remove them from the image since the method is primarily designed to differentiate the texture and structure signals. Note that this step plays a different role compared with our previous step, which utilizes RTV prior as a penalty term. The difference is illustrated in Fig. 1.

Cho et al. [12] suggested that the artifacts result from edge blurring. Therefore, we further employ the shocking filter to enhance the remaining edges after salient edges have been selected, which is to reduce the influence of the blur. Farbman et al. [19] suggested that sharpening also leads to halos and gradient reversals. Thus, we limit the degree of shocking to recover the authentic edge information at utmost.

The model of selecting the salient edge could be expressed as:

$$X = \phi(\arg\min_S \Sigma_p \left(S_p - I_p\right)^2 + \lambda_s\left(\frac{D_x(p)}{L_x(p)+\varepsilon} + \frac{D_y(p)}{L_y(p)+\varepsilon}\right)) \tag{13}$$

Where S denotes the salient edge image produced by applying additional RTV to the intermediate image x; $\phi(\cdot)$ represents the shocking filter; λ_s controls the degree of smooth; σ_s is the scale size of the window; and X is the final salient edge image.

3.3 Kernel Estimation

Many previous algorithms, including [9, 10, 12], employ a simple Gaussian prior to estimate the kernel. They believe that it is of great efficiency to do so based on the assumption that the latent image x estimation has guaranteed the accuracy of the model. However, it is a misunderstanding that the prediction step is enough to reduce the noise and ringing artifacts in the estimation process. Another group of people pointed out that many kernels are highly non-Gaussian, they instead try to seek a mixture of sparse priors to force the kernel to fit into the natural statistics, including [11, 13, 15, 21]. Among these algorithms, we find that the bi-L0-L2 method [11] is the most suitable one where the sparse L0 prior and the Gaussian prior is imposed together on the kernel, thus it can not only apply to the Gaussian kernel but also other circumstances. Moreover, the blur kernel is estimated in the derivative domain, which is found useful to suppress the noise.

Following [11], the blur kernel is estimated by solving

$$k_{i+1} = \arg\min_k \lambda \|k * x_i - y\|^2 + C_k^i \alpha_k (\|k\|_0 + \frac{\beta_k}{\alpha_k} \|k\|^2) \tag{14}$$

where $0 \leq i \leq Q - 1$, Q is the inner iteration number; β_k is a weight parameter; $\|\cdot\|_0$ denotes the L0-semi norm; and $C_k^i < 1$ is a positive continuation factor which is fixed as 4/5. Then k could be efficiently solved by OSAL in the same manner as x in (5)–(12).

To remove noise, we also impose a threshold on the kernel. Besides, we set negative elements to zero and normalize the kernel. In addition to this, we compute the connected components in the image to remove areas without enough components, following the idea in [17].

4 Image Recovery

Once the kennel is estimated at the finest scale, the blind deconvolution turns into a non-deconvolution. Numerious methods have been employed to address this classical scheme. However, early algorithms like Richardson-Lucy (RL) and mixture of Gaussians [1] are sensitive to kernel noise. We notice that the Hyper-Laplacian prior [4] strikes a balance between accuracy and speed. It relies on heavy-tailed natural image priors and look-up tables, which render it a comparative advantage over the other non-blind deconvolution methods. The prior has then be adopted by many papers [8–11, 21] afterwards. However, there is still some noise and artifacts left.

We employ a smoothness prior [22] developed from the Hyper-Laplacian prior [4]. The new prior makes use of the canny operator to locate the edges. Then it dilates the detected edges with a disk model. The objective function is defined as (15):

$$\min_x \lambda \|k_i * x - y\|^2 + \lambda_1 \|\nabla x\|^{0.5} \circ M + \lambda_2 \|\nabla x\|^2 \circ (J - M) \tag{15}$$

where $\nabla x = (\partial_x x, \partial_y x)^T$ is the gradient of the image x; λ_1 and λ_2 are the weights; J is an all-ones matrix and M is a mask. The parameter setting follows the idea in [4, 22].

5 Experimental Details and Results

In this section, we present the experimental evaluations of our proposed method on both synthetic and real image datasets [5] compared with the state-of-the-art approaches. All of our experiments are carried out on a laptop with an Intel i7-5500U processer and 8 GB RAM. A 255 * 255 image takes about 2 min to process on Matlab. In order to get better performance, we set the outer and inner iteration number to be 16 and 14 respectively at each scale. Moreover, $\lambda = 100$, $\alpha_x = 0.55$, $\gamma_x = 200$, $\sigma = 3$ in

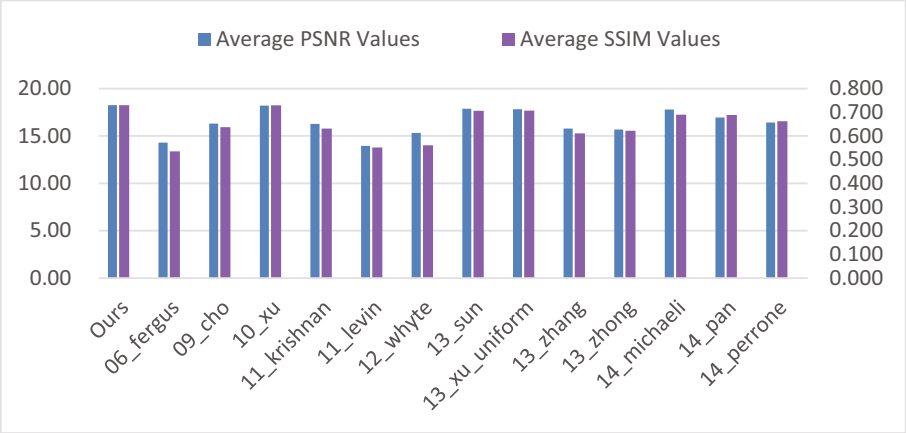

Fig. 2. Quantitative comparison on the synthetic dataset [5]. Our method and Xu and Jia [13] have a comparative advantage over the others on the SSIM and PSNR values.

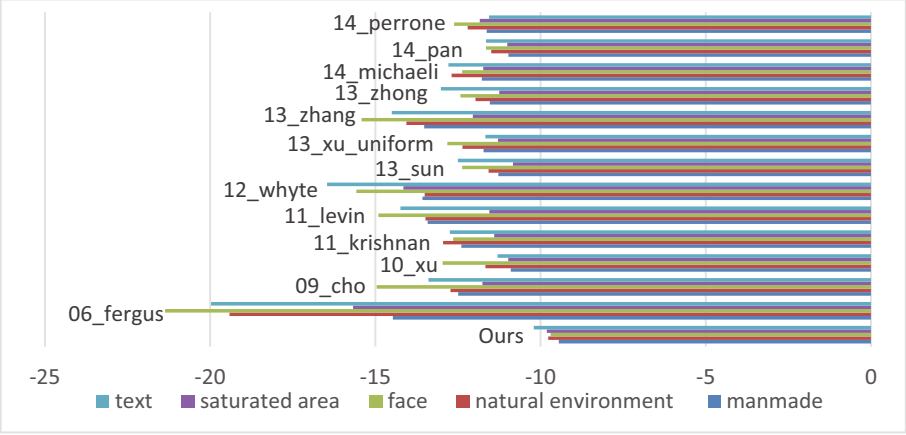

Fig. 3. Quantitative comparison on the synthetic dataset [5] measured by [6]. The larger value represents better performance. Our method outperforms in all five categories.

the intermittent image estimation. In the next stage of edge selection, the initial values of σ_s and λ_s are set to 1.5 and 0.02, respectively. We then gradually enhance the smooth effect by increasing them 1.1 times. Finally, we set $\alpha_k = 0.25$ in the kernel estimation empirically.

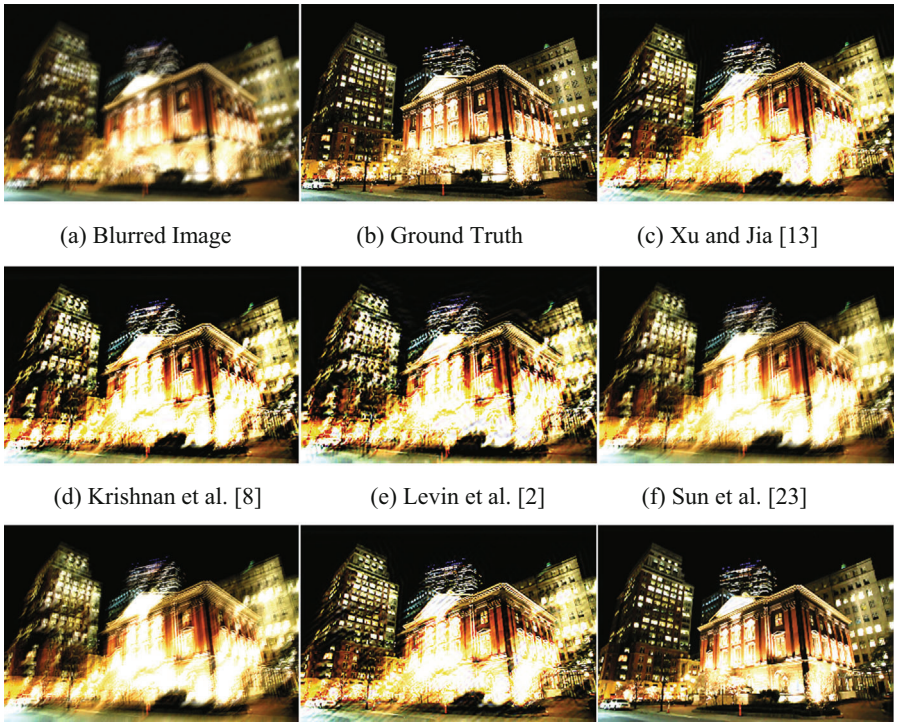

(a) Blurred Image (b) Ground Truth (c) Xu and Jia [13]

(d) Krishnan et al. [8] (e) Levin et al. [2] (f) Sun et al. [23]

(g) Xu et al. [9] (h) Pan et al. [10] (i) Ours

Fig. 4. Deblurred results of an image with saturated area. We showed the top 7 of all 14 methods. The metric's [6] scores of (c)–(i) are −11.84, −12.01, −12.50, −12.13, −12.38, −11.74 and −10.09, respectively. (d) and (g) fail to accurately restore the image because of the saturated area. (c), (e), (f) and (h) have varying degrees of ringing artifacts while ours gets superior result.

Synthetic Images. We run our algorithm on the synthetic dataset [5]. It contains 25 images, divided into 5 categories including some particular circumstances such as natural environment, text, face and saturation. We compare our SSIM and PSNR results with Fergus et al. [1], Cho et al. [12], Xu and Jia [13], Krishnan et al. [8], Levin et al. [2], Whyte et al. [15], Sun et al. [23], Xu et al. [9], Zhang et al. [24], Zhong et al. [25], Michaeli and Irani [26], Pan et al. [10], and Perrone et al. [27]. The average PSNR values are shown in Fig. 2.

Although SSIM and PSNR are the most popular metrics to measure a deblurring method, it cannot always faithfully reflect the performance of the methods since people's eyes may have different feelings not matched with the value. To be more

specific, human visual system is influenced by many factors, for example, the surrounding area will affect people's evaluation on the target area. Thus, we adopt a no-reference metric [6], which is learned based on a massive user study. It can score image quality and artifacts consistently with human ratings. The results are illustrated in Fig. 3.

It is clearly observed that all of the previous state-of-the-art methods could not be considered as robust algorithms. There are always some scenarios where they perform badly or just completely fail. However, the proposed method has achieved universally better restoration performance across the five categories of images. Figures 4 and 5 demonstrate two examples, i.e., images with saturated area and text.

Fig. 5. Deblurred results of a text image. The left is the input blurry image; the middle and right are cropped regions from the input. (a)–(h) are Xu and Jia [13], Krishnan et al. [8], Sun et al. [23], Zhong et al. [25], Michaeli and Irani [26], Pan et al. [8], Perrone et al. [27], and Ours, respectively. We can see that our text results have less artifacts and are easy to recognize.

Real Images. Here we compare our method with the state-of-the-art algorithms on two real photographs [5]. Figure 6 shows the deblurring results on the real photograph fish for visual comparison. We can see that Fig. 6(d) and (h) have severe ringing artifacts. Figure 6(b), (c) and (e) have a sense of smoothness in which details are blurry. Comparatively, the results of Pan et al. [10] and our method are most visually pleasing. Figure 7 shows another group of results which also demonstrates the comparative performance of the proposed approach to other methods.

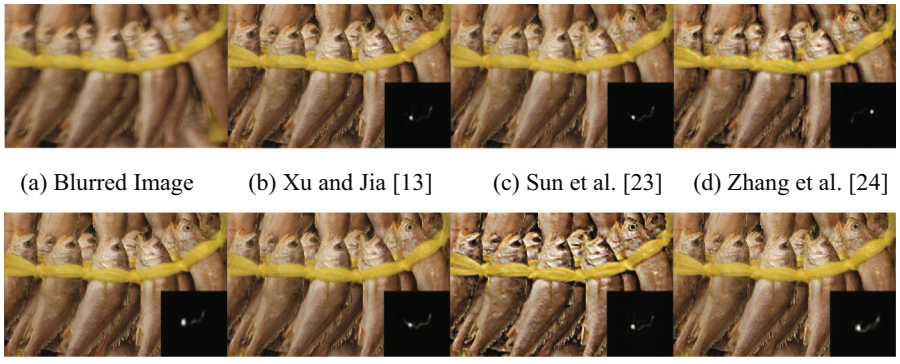

(a) Blurred Image (b) Xu and Jia [13] (c) Sun et al. [23] (d) Zhang et al. [24]

(e) Zhong et al. [25] (f) Pan et al. [10] (h) Perrone et al. [27] (i) Ours

Fig. 6. Deblurring results on the real photograph of fishes.

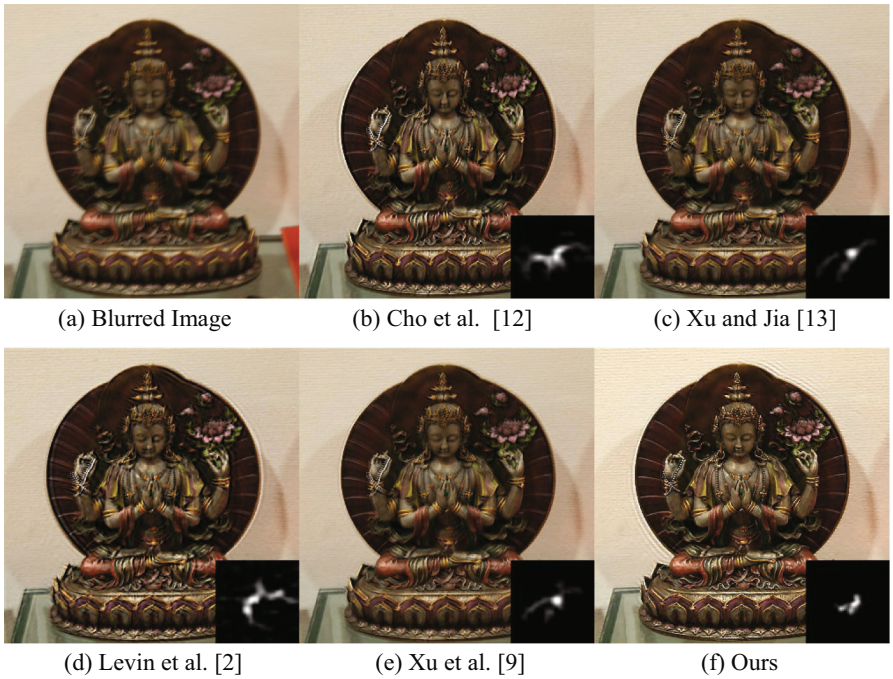

(a) Blurred Image (b) Cho et al. [12] (c) Xu and Jia [13]

(d) Levin et al. [2] (e) Xu et al. [9] (f) Ours

Fig. 7. Deblurring results on the real photograph statue. As we can see from the details and the estimated kernels, our algorithm has a superior performance over the state-of-the-art methods.

6 Conclusion

In this paper, we propose a robust blind deconvolution approach with RTV as a regularization penalty, which is easily solved by applying the OSAL (operator splitting and the augmented Lagrangian) scheme. Extensive experiments on a challenging synthetic dataset and real-world images as well are conducted to validate the new approach with comparison against the state-of-the-art approaches from 2006 to 2014. Based on both PSNR and SSIM and a non-reference evaluation metric, the results demonstrate that the new approach is comparatively more effective to process blurred images in more challenging cases including images with text, low illumination and face.

Acknowledgement. The research was supported in part by the Natural Science Foundation (NSF) of China (61771250, 61402239).

References

1. Fergus, R., Singh, B., Hertzmann, A., Roweis, S.T., Freeman, W.T.: Removing camera shake from a single photograph. ACM Trans. Graph. **25**(3), 787–794 (2006)
2. Levin, A., Weiss, Y., Durand, F., Freeman, W.T.: Understanding blind deconvolution algorithms. IEEE Trans. Pattern Anal. Mach. Intell. **33**(12), 2354 (2011)
3. Xu, L., Yan, Q., Xia, Y., Jia, J.: Structure extraction from texture via relative total variation. ACM Trans. Graph. **31**(6), 139 (2012)
4. Krishnan, D., Fergus, R.: Fast image deconvolution using hyper-Laplacian priors. In: International Conference on Neural Information Processing Systems, pp. 1033–1041. Curran Associates Inc. (2009)
5. Lai, W.S., Huang, J.B., Hu, Z., Ahuja, N., Yang, M.H.: A comparative study for single image blind deblurring. In: IEEE Conference on Computer Vision and Pattern Recognition, pp. 1701–1709. IEEE Computer Society (2016)
6. Liu, Y., Wang, J., Cho, S., Finkelstein, A., Rusinkiewicz, S.: A no-reference metric for evaluating the quality of motion deblurring. ACM Trans. Graph. **32**(6), 175 (2013)
7. Shan, Q., Jia, J., Agarwala, A.: High-quality motion deblurring from a single image. ACM Trans. Graph. **27**(3), 1–10 (2008)
8. Krishnan, D., Tay, T., Fergus, R.: Blind deconvolution using a normalized sparsity measure. Comput. Vis. Pattern Recogn. **42**, 233–240 (2011). IEEE
9. Xu, L., Zheng, S., Jia, J.: Unnatural L0 sparse representation for natural image deblurring. Comput. Vis. Pattern Recogn. **9**, 1107–1114 (2013). IEEE
10. Pan, J., Hu, Z., Su, Z., Yang, M.H.: Deblurring text images via L0-regularized intensity and gradient prior. In: IEEE Conference on Computer Vision and Pattern Recognition, pp. 2901–2908. IEEE Computer Society (2014)
11. Shao, W.-Z., Li, H.-B., Elad, M.: Bi-l0-l2-norm regularization for blind motion deblurring. J. Vis. Commun. Image Represent. **33**, 42–59 (2015)
12. Cho, S., Lee, S.: Fast motion deblurring. ACM Trans. Graph. **28**(5), 1–8 (2009)
13. Xu, L., Jia, J.: Two-phase kernel estimation for robust motion deblurring. In: Daniilidis, K., Maragos, P., Paragios, N. (eds.) ECCV 2010. LNCS, vol. 6311, pp. 157–170. Springer, Heidelberg (2010). https://doi.org/10.1007/978-3-642-15549-9_12
14. Pan, J., Lin, Z., Su, Z., Yang, M.H.: Robust kernel estimation with outliers handling for image deblurring. In: IEEE Conference on Computer Vision and Pattern Recognition, pp. 2800–2808. IEEE Computer Society (2016)
15. Whyte, O., Sivic, J., Zisserman, A., Ponce, J.: Non-uniform deblurring for shaken images. Int. J. Comput. Vis. **98**(2), 168–186 (2012)
16. Hu, Z., Yang, M.-H.: Good regions to deblur. In: Fitzgibbon, A., Lazebnik, S., Perona, P., Sato, Y., Schmid, C. (eds.) ECCV 2012. LNCS, vol. 7576, pp. 59–72. Springer, Heidelberg (2012). https://doi.org/10.1007/978-3-642-33715-4_5
17. Hu, Z., Cho, S., Wang, J., Yang, M.H.: Deblurring low-light images with light streaks. In: IEEE Conference on Computer Vision and Pattern Recognition, pp. 3382–3389. IEEE Computer Society (2014)
18. Pan, J., Sun, D., Pfister, H., Yang, M.H.: Blind image deblurring using dark channel prior. In: IEEE Conference on Computer Vision and Pattern Recognition, pp. 1628–1636. IEEE Computer Society (2016)
19. Farbman, Z., Fattal, R., Lischinski, D.: Edge-preserving decompositions for multi-scale tone and detail manipulation. ACM Trans. Graph. **27**(3), 1–10 (2008)
20. Xu, L., Lu, C., Xu, Y., Jia, J.: Image smoothing via L0, gradient minimization. In: SIGGRAPH Asia Conference, vol. 30, p. 174. ACM (2011)

21. Krishnan, D., Bruna, J., Fergus, R.: Blind deconvolution with non-local sparsity reweighting. In: Computer Science (2013)
22. Zhang, X., Wang, R., Tian, Y., Wang, W., Gao, W.: Image deblurring using robust sparsity priors. In: IEEE International Conference on Image Processing, pp. 138–142. IEEE (2015)
23. Sun, L., Cho, S., Wang, J., Hays, J.: Edge-based blur kernel estimation using patch priors. In: IEEE International Conference on Computational Photography, vol. 6, pp. 1–8. IEEE (2013)
24. Zhang, H., Wipf, D., Zhang, Y.: Multi-image blind deblurring using a coupled adaptive sparse prior. In: IEEE Conference on Computer Vision and Pattern Recognition, vol. 9, pp. 1051–1058. IEEE Computer Society (2013)
25. Zhong, L., Cho, S., Metaxas, D., Paris, S., Wang, J.: Handling noise in single image deblurring using directional filters. In: IEEE Conference on Computer Vision and Pattern Recognition, vol. 9, pp. 612–619. IEEE Computer Society (2013)
26. Michaeli, T., Irani, M.: Blind deblurring using internal patch recurrence. In: Fleet, D., Pajdla, T., Schiele, B., Tuytelaars, T. (eds.) ECCV 2014. LNCS, vol. 8691, pp. 783–798. Springer, Cham (2014). https://doi.org/10.1007/978-3-319-10578-9_51
27. Perrone, D., Favaro, P.: Total variation blind deconvolution: the devil is in the details. In: IEEE Conference on Computer Vision and Pattern Recognition, pp. 2909–2916. IEEE Computer Society (2014)